SST and circulation trend biases cause an underestimation of European precipitation trends

Ronald van Haren · Geert Jan van Oldenborgh · Geert Lenderink · Matthew Collins · Wilco Hazeleger

Abstract Clear precipitation trends have been observed in Europe over the past century. In winter, precipitation has increased in north-western Europe. In summer, there has been an increase along many coasts in the same area. Over the second half of the past century precipitation also decreased in southern Europe in winter.

An investigation of precipitation trends in two multi-model ensembles including both global and regional climate models shows that these models fail to reproduce the observed trends. In many regions the model spread does not cover the trend in the observations.

In contrast, regional climate model (RCM) experiments with observed boundary conditions reproduce the observed precipitation trends much better. The observed trends are largely compatible with the range of uncertainties spanned by the ensemble, indicating that the boundary conditions of RCMs are responsible for large parts of the trend biases. We find that the main factor in setting the trend in winter is atmospheric circulation, for summer sea surface temperature (SST) is important in setting precipitation trends along the North Sea and Atlantic coasts. The causes of the large trends in atmospheric circulation and summer SST are not known. For SST there may be a connection with the well-known ocean circulation biases in low-resolution ocean models. A quantitative understanding of the causes of these trends is needed so that climate model based projections of future climate can be corrected for these precipitation trend biases.

Keywords Europe · precipitation · trends · climate models · observations · uncertainty

1 Introduction

A wide range of studies have shown that increases in atmospheric CO_2 concentrations and other greenhouse gasses influence the climate, affecting many variables (Hegerl and Zwiers, 2011). Projections of future climate based on these studies are uncertain (e.g. Déqué et al., 2007; Räisänen, 2007; Hawkins and Sutton, 2009; Knutti et al., 2009). To have confidence in future climate projections, a correct representation of trends in the past is necessary (but not sufficient). In this paper we consider the uncertainty in one variable and one region: European precipitation trends.

Simulations of present and future climate are typically done using climate models. Climate models are a mathematical representation of the climate system and should in principle give a physics-based response to increased CO_2 concentrations and changes in other forcings. However, projections also depend on uncertain parameterizations of unresolved processes that are used in climate models, uncertainty about land use and the magnitude of forcings due to aerosol and black carbon emissions. Part of this uncertainty is described by the spread of multi-model and perturbed physics ensembles. In this paper we investigate whether the ensemble spread indeed covers the observed precipitation trends in Europe.

R. van Haren (✉) · G.J. van Oldenborgh · G. Lenderink · W. Hazeleger
Royal Netherlands Meteorological Institute (KNMI), De Bilt, The Netherlands
E-mail: ronald.van.haren@knmi.nl

M. Collins
University of Exeter, Exeter, United Kingdom

W. Hazeleger
Meteorology and Air Quality Section, Wageningen University, Wageningen, The Netherlands

Previous studies have shown a tendency for climate model ensembles to underestimate precipitation trends (Wentz et al., 2007; Zhang et al., 2007; Bhend and von Storch, 2008). Over Europe, local weather variations are to a large extent determined by changes in circulation (Osborn et al., 1999; Turnpenny et al., 2002; van Oldenborgh and van Ulden, 2003; van Ulden and van Oldenborgh, 2006), but also changes in sea surface temperature (SST) are known to be responsible for precipitation variations on different spatial scales (Rowell, 2003; van Ulden and van Oldenborgh, 2006; Kjellström and Ruosteenoja, 2007; Lenderink et al., 2009). Modeled trends in atmospheric circulation (Osborn, 2004; van Oldenborgh et al., 2009a) and SST (van Oldenborgh et al., 2009a; Ashfaq et al., 2010) contain large biases and could be responsible for the underestimation of precipitation trends.

We evaluate modeled precipitation trends in a few different climate model ensembles. First we compare observed precipitation trends with trends from the CMIP3 ensemble of climate model experiments (Meehl et al., 2007), an ensemble composed of Global Circulation Models (GCMs). Searching for causes of the difference in trends, we discuss trend differences between the CMIP3 ensemble and an ensemble of regional climate models (RCMs). RCMs are a dynamical downscaling tool and provide more details on local conditions such as surface conditions, topography, coastlines and soil moisture that could affect modeled precipitation. RCMs are constrained by the lateral boundaries, and it is therefore relatively straightforward to prescribe circulation. For GCMs this is much more difficult (van der Schrier and Barkmeijer, 2007). Also SST is commonly prescribed in RCM simulations. We use this property to compare the RCM results with the results of a similar set of RCMs forced by prescribed quasi-observed circulation and SST. This allows for a separation between errors in lateral boundary conditions and internal model errors (Hudson and Jones, 2002). Trend biases that exist in both RCM ensembles are ascribed to model errors, whereas trend biases only found in the GCM driven RCM ensemble are ascribed to errors in the boundary conditions, large scale atmospheric circulation and SST. Finally, we try to separate these two factors using a statistical analysis.

2 Data and preprocessing

2.1 Trend definition

We use the common definition of a trend in this paper, regression against time. Previous studies have shown that the magnitude of regional climate changes increases quasi-linearly with changes in the global mean temperature (Räisänen, 2007; Alexander and Arblaster, 2009), a definition adopted in e.g. van Oldenborgh et al. (2009a). Although the latter definition may physically be better justified, it did not significantly increase the signal-to-noise ratio, nor did it affect any of the conclusions. We therefore adopted the former, more common, approach in this paper. As a result the trend is highly dependent on the chosen time interval: because global warming has not been linear with time, the trends over the last century are smaller than over the last 50 years.

We consider precipitation trends separately for the summer (April – September) and winter (October – March) half year. This increases the signal to noise ratio compared to a three monthly definition of the summer and winter period. In order to compare wet and dry regions in a single figure, we use relative precipitation trends in this paper. The relative precipitation trend is related to the absolute precipitation trend by

$$P'(x,y) = \frac{P'_{abs}(x,y)}{\overline{P(x,y)}} \quad (1)$$

where $P'_{abs}(x,y)$ is the absolute precipitation trend and $\overline{P(x,y)}$ is the mean seasonal (summer/winter) precipitation over the period that the trend is computed. Relative precipitation trends are further referred to as precipitation trends, or just trends.

2.2 Observations

We use four observational datasets in this study to evaluate the model results. First the low (2.5°) resolution gridded precipitation dataset of the Global Precipitation Climatology Centre (Schneider et al., 2010, GPCC v5 (1901 - 2009)) is used for comparison with the results derived from a large multi-model GCM ensemble. Later the state-of-the-art gridded high (0.5°) resolution precipitation fields of the European ENSEMBLES project (Haylock et al., 2008, E-OBS v5.0 (1951 - 2011)) is used to verify the results derived from RCM ensembles. We also used the precipitation dataset from the Climate Research Unit (Mitchell and Jones, 2005, CRU TS3.10 (1901 - 2009)), as well as the high resolution GPCC v5 dataset (0.5°), to verify the quality of the observational datasets.

It is well known that observations are affected by many sources of error. Errors stem from sources of uncertainty in the observational data and their analysis, from measurement, recording and representativity errors to data quality, homogeneity and interpolation errors (Haylock et al., 2008). Haylock et al. (2008) claim that the typical interpolation error is much larger than

the expected magnitude of other sources of uncertainty. To investigate the uncertainty we compare the three observational sets as well as the ERA-40 re-analysis. This is done for the common time period where all datasets and model results have data (1961 – 2000, figure 1). We also show the absolute summer and winter precipitation trends in figure 2.

The summer precipitation trend found for the ERA-40 dataset differs largely from the trends found for the observational datasets. Largest deviations are mainly found for central Europe, but also for other European regions in the summer half year. The relatively small amount of wind-induced undercatch (difference between the actual amount of precipitation and the amount measured by a precipitation gauge) during the summer and the high number of measurement stations in this area make it likely that the observational datasets give a better representation of the actual trend. We will therefore not consider the ERA-40 precipitation trends any further in this paper.

As a measure of uncertainty we compute for each grid point the standard deviation between the trend fields of the different observational datasets (panels (e,j) of figure 1) according to

$$
\sigma = \sqrt{\frac{1}{N} \sum_{i=1}^{N} \left(P'\left(x,y\right)_i - \mu \right)^2},
$$

$$
\text{with} \quad \mu = \frac{1}{N} \sum_{i=1}^{N} P'(x,y)_i
$$

(2)

in which $P'\left(x,y\right)_i$ are the relative precipitation trends as given by panels (b–d) and (g–i) of figure 1 and N is the number of observational datasets. Note that this samples only part of the uncertainty as the datasets are based on a subset of the same station data. Inhomogeneities in the underlying station data propagate into all observational datasets. Inhomogeneities could be caused by e.g. a drop in ratio of snow to liquid rainfall (Hundecha and Bárdossy, 2005) or changes in measuring arrangements.

We find considerable differences between the observational datasets over Greece, Finland, the former Soviet Union and the Iberian peninsula (both seasons) and France and the Scandinavian peninsula (winter half year). Differences on smaller spatial scales are found in many other areas. We will only consider model ensemble trend biases larger than the difference between the different observational datasets.

2.3 Model ensembles

We use three multi-model ensembles in this study: one composed of GCMs and two composed of RCMs. The GCM composed ensemble used is the Coupled Model Intercomparison Project phase 3 (Meehl et al., 2007, CMIP3) multi-model ensemble from the World Climate Research Programme (WCRP). The CMIP3 dataset consists of 23 models (left column of figure 3) at varying spatial resolution, typically in the order of 200 km. For the period before 2000 we use the climate of the 20th century runs (20c3m). For the period after 2000 we use the SRES A1b scenario runs, but it should be noted that the other SRES emission scenarios are almost identical for the short period after 2000 that is used in this study.

For the ensembles composed of RCMs we use those provided by Research Theme 2b (RT2b) and Research Theme 3 (RT3) from the European ENSEMBLES project (van der Linden and Mitchell, 2009), interpolated on a regular 0.5° longitude-latitude grid. The main difference between the two RCM ensembles is the forcing at the boundaries; the regional models are fed at their boundaries with fields containing temperature, humidity, horizontal winds and surface pressure. The fields are commonly provided each 6 hours from the GCMs (RT2b) or ERA-40 (RT3), and are linearly interpolated in time. The boundary relaxation zone in the regional models is typically 8-16 grid points wide, and relaxation is done with a short time scale (in the order of the typical time step of the model) at the outer relaxation zone and a longer time scale at the inner relaxation zone. The exact way this is done varies between the models. SSTs are prescribed from the GCMs or ERA-40.

An overview of the models used in this analysis from the RT2b ensemble is given in the right column of figure 3. Most model data used in the two ensembles is available at a 25 km spatial resolution. Exceptions are the MIROC3.2hires forced RACMO (KNMI) model in the RT2b ensemble and the CLM (GKSS) model in the RT3 ensemble that are only available at a 50 km resolution. Models that were excluded in this analysis were either not available for the complete 1951-2009 time period or for the complete European domain. The models used from the RT3 ensemble are mostly the same as those used from the RT2b ensemble. However, we re-added the CLM (GKSS) model that we removed from the RT2b ensemble because it was not available for the complete time period. We also excluded the PROMES (UCLM) model from the RT3 ensemble because the spatial noise in the computed trend was found to be unrealistic.
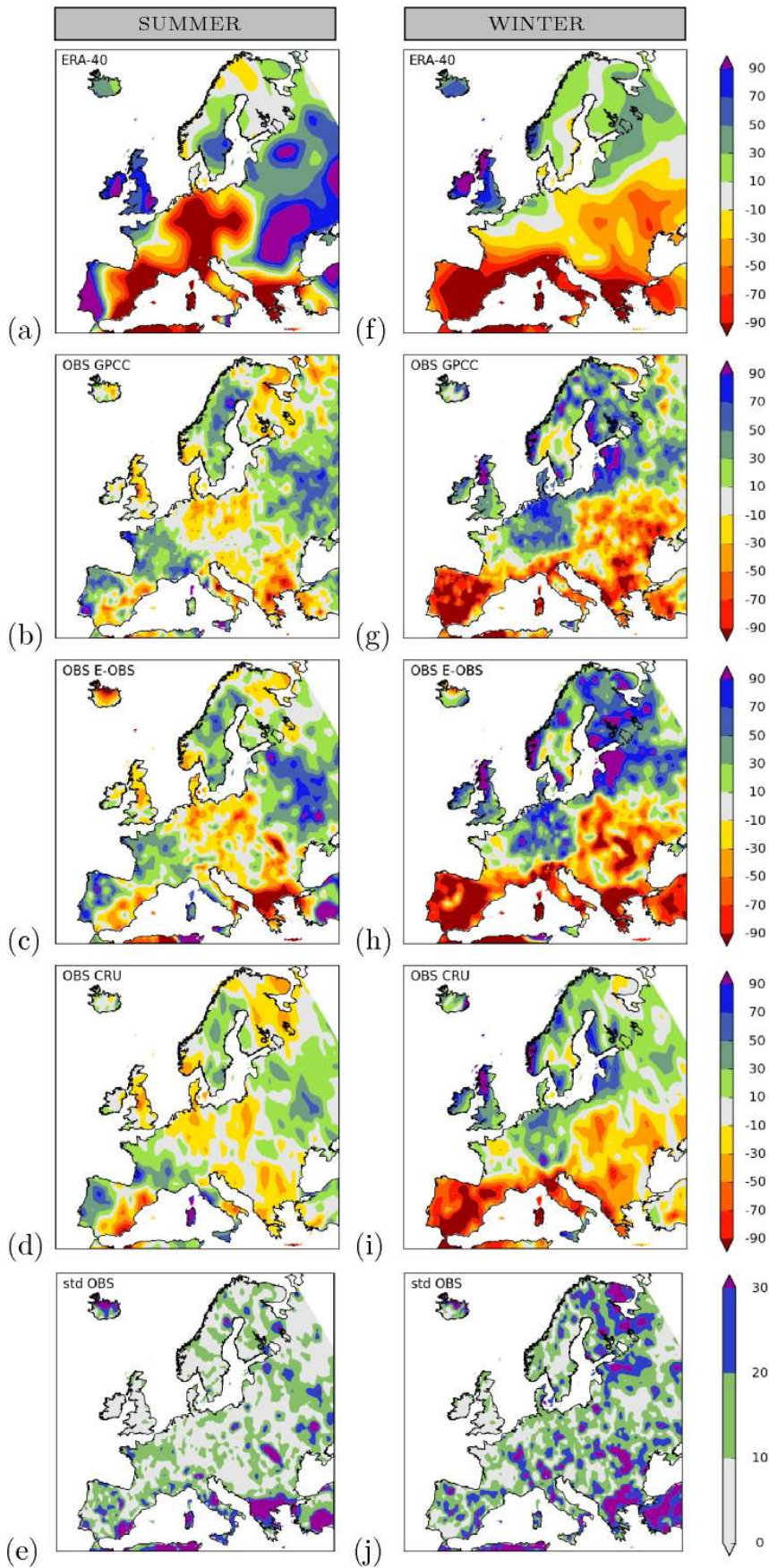
Fig. 1 Comparison of ERA-40 and observed precipitation trends over 1961-2000, defined as the regression against time. (a) Relative trends in ERA-40 summer precipitation [%/Century] (b) Relative trends in GPCC summer precipitation [%/Century] (c) Relative trends in E-OBS summer precipitation [%/Century] (d) Relative trends in CRU summer precipitation [%/Century] (e) Standard deviation between GPCC, CRU and E-OBS trends summer (f–j) Same but for winter precipitation.
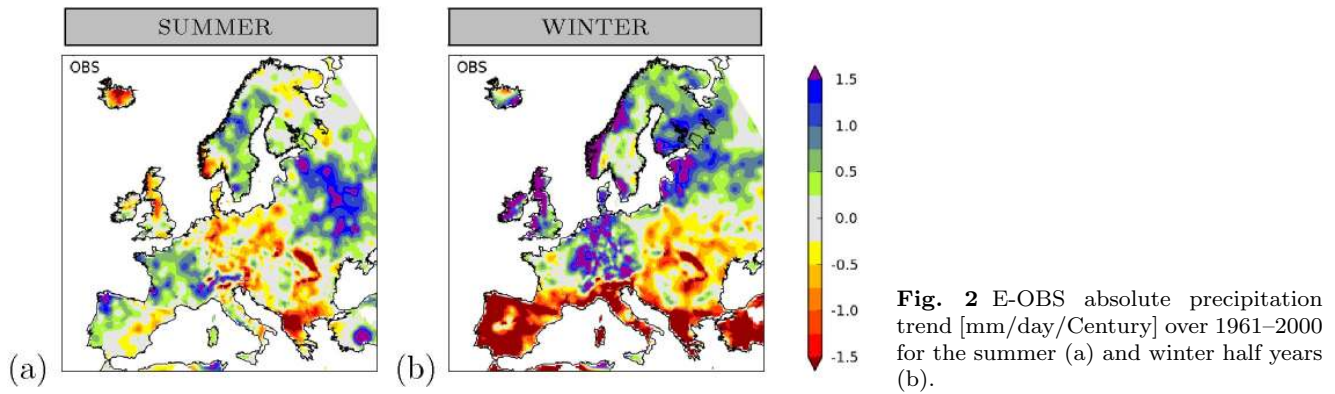
Fig. 2 E-OBS absolute precipitation trend [mm/day/Century] over 1961–2000 for the summer (a) and winter half years (b).

3 GCM/RCM trends vs observations

3.1 GCM simulations

Precipitation trends for the GCM and GCM forced RCM multi-model ensembles are computed as regression against time. In order to be least affected by natural variability we used the largest common period for the model ensembles and the observations, yielding 1901 - 2009 for the GCM ensemble and the GPCC precipitation data, and 1951 - 2009 for the GCM forced RCM ensemble and the E-OBS precipitation data. The results for the GCM forced RCM ensemble are also shown for the shorter 1961 - 2000 period, the common period shared with the ERA-40 forced RCM ensemble.

The comparison between each multi-model ensemble and the observational data is two-fold. First the trend of the ensemble mean is compared to the trend in the observational data. Next we verify if the observational trends fall within the bandwidth of natural variability combined with model uncertainty as parameterized by the spread of the multi-model ensemble. This is indicated by the fraction of the model ensemble members with a trend larger than the observed one.

Figure 4 shows the results for the GCM ensemble and the GPCC observational dataset. Whereas the observations show clear positive trends in northern Europe (both seasons) and part of western Europe (both seasons), these are much smaller in the GCM ensemble. Panels (d,i) of figure 4 show that the model spread in these areas does not cover the observations. Similar results are obtained when using the CRU observational dataset at a resolution of 2.5°.

As an aggregated statistic we computed the Talagrand diagram or rank histogram over the land area of Europe and show them in panels (e,j) of figure 4. At every grid point the N ensemble members are ranked from lowest to highest, representing N+1 possible bins in which the observations could fall (including the extremes). For every grid point the bin in which the observed trend falls is identified and recorded and the histogram is built up over all area-weighted grid points. For a *reliable* ensemble the histogram would be flat. If the model ensemble has a trend bias, a larger part of the area lies at one end of the ensemble spread, i.e., that end of the histogram will curve up. Because of large uncertainties in the observations in especially Greece and Finland (panels (e,j) of figure 1) we only considered the area west of these two countries (west of 20° longitude). Different observational estimates are used to compute the histograms to give some indication of uncertainties in the observations. In figure 4 the blue and red lines curve up at the low fractions indicating a bias towards less wetting and more drying trends in the models compared to the observations.

The next question is whether the bias is significant, i.e., whether it is unlikely to be a fluctuation in the distribution of model spread and natural variability. The strong correlation between neighboring grid points is a major issue when conducting significance tests. We therefore take the correlation as represented in the RCMs into account when constructing the significance intervals for each bin in the Talagrand diagrams. All bins have a common scale by design; between 0 and 1. To compute significance intervals around the flat line we compute the same histogram considering each model in turn to be the 'truth' (Annan and Hargreaves, 2010). The confidence interval, depicted as the gray bars in panels (e,j) of figure 4, is constructed as the distance between 0 (the minimum) and the second highest ranked member for each bin. This gives, under the assumption that the members are equally distributed over the N+1 inter-point intervals of the empirical distribution function (including the two beyond the minimum and maximum sample values), a confidence interval of around 90% (1-sided test).

We find that the bias in reproducing wetting trends is significant at the 90% confidence level, both in the summer and winter half years. The bias in reproducing drying trends in the winter is not significant. From this
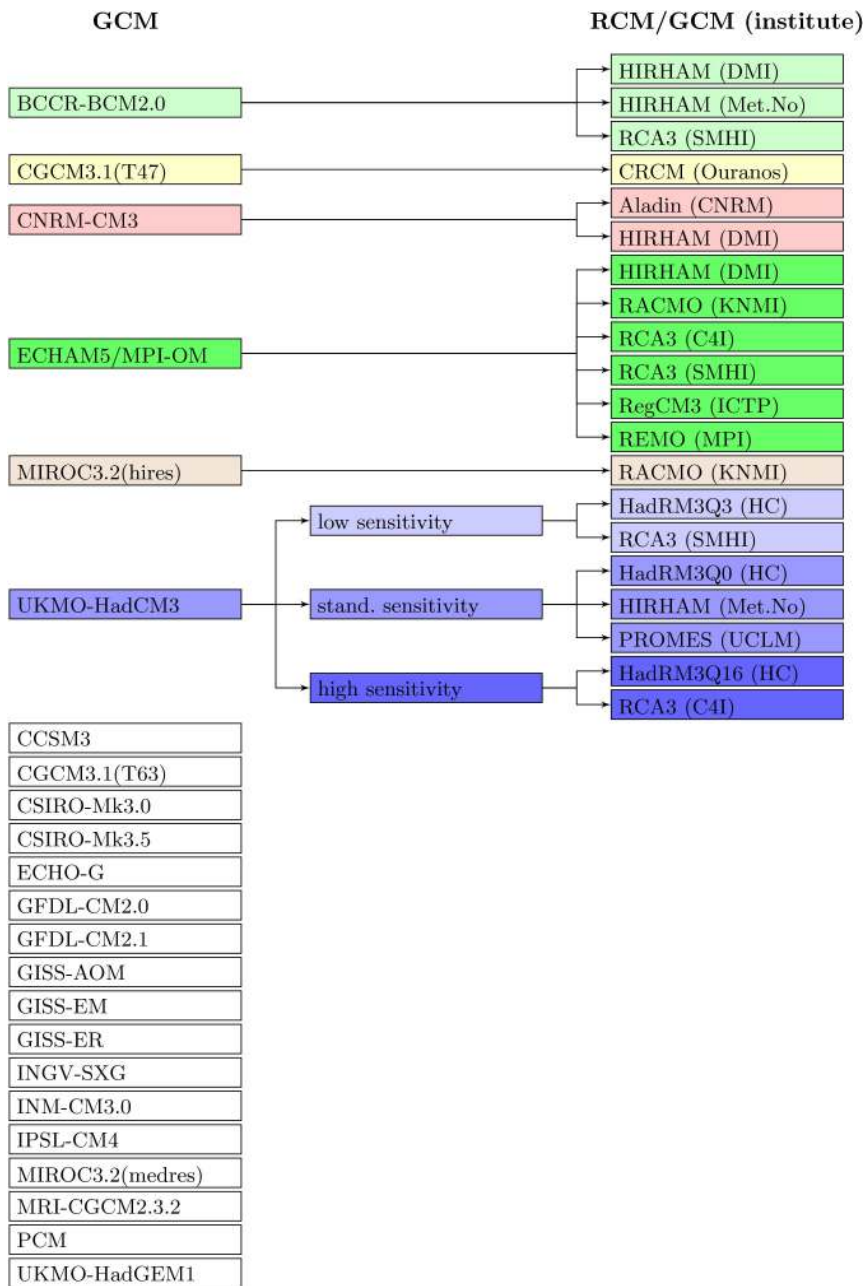
GCM   **RCM/GCM (institute)**

BCCR-BCM2.0	HIRHAM (DMI)
	HIRHAM (Met.No)
	RCA3 (SMHI)
CGCM3.1(T47)	CRCM (Ouranos)
CNRM-CM3	Aladin (CNRM)
	HIRHAM (DMI)
	HIRHAM (DMI)
	RACMO (KNMI)
ECHAM5/MPI-OM	RCA3 (C4I)
	RCA3 (SMHI)
	RegCM3 (ICTP)
	REMO (MPI)
MIROC3.2(hires)	RACMO (KNMI)

UKMO-HadCM3 — low sensitivity → HadRM3Q3 (HC), RCA3 (SMHI)

stand. sensitivity → HadRM3Q0 (HC), HIRHAM (Met.No), PROMES (UCLM)

high sensitivity → HadRM3Q16 (HC), RCA3 (C4I)

CCSM3
CGCM3.1(T63)
CSIRO-Mk3.0
CSIRO-Mk3.5
ECHO-G
GFDL-CM2.0
GFDL-CM2.1
GISS-AOM
GISS-EM
GISS-ER
INGV-SXG
INM-CM3.0
IPSL-CM4
MIROC3.2(medres)
MRI-CGCM2.3.2
PCM
UKMO-HadGEM1

Fig. 3 Overview of GCMs and GCM forced RCMs used in the analysis.

we conclude that the problem appears to be a bias in the trends and not in the width of the ensemble: the low and high ranks are not symmetric but the trend in the observations is systematically larger than the trend in the models. This shows that the trend in the observations does not fall within the bandwidth of natural variability combined with model uncertainty as parameterized by the spread of the multi-model ensemble.

3.2 RCM simulations

To investigate whether the observed trend biases are due to the coarse resolution of GCMs, we considered a large multi-model RCM ensemble forced by boundary conditions derived from GCM simulations (RCM/GCM). Figure 5 shows the results for the RCM/GCM ensemble for the period 1951-2009. Figure 6 shows the same but for the period 1961-2000. The available time periods for the RCM/GCM ensemble are considerably shorter compared to the GCM ensemble. As a result the observed trends and trend mismatches are harder to de-
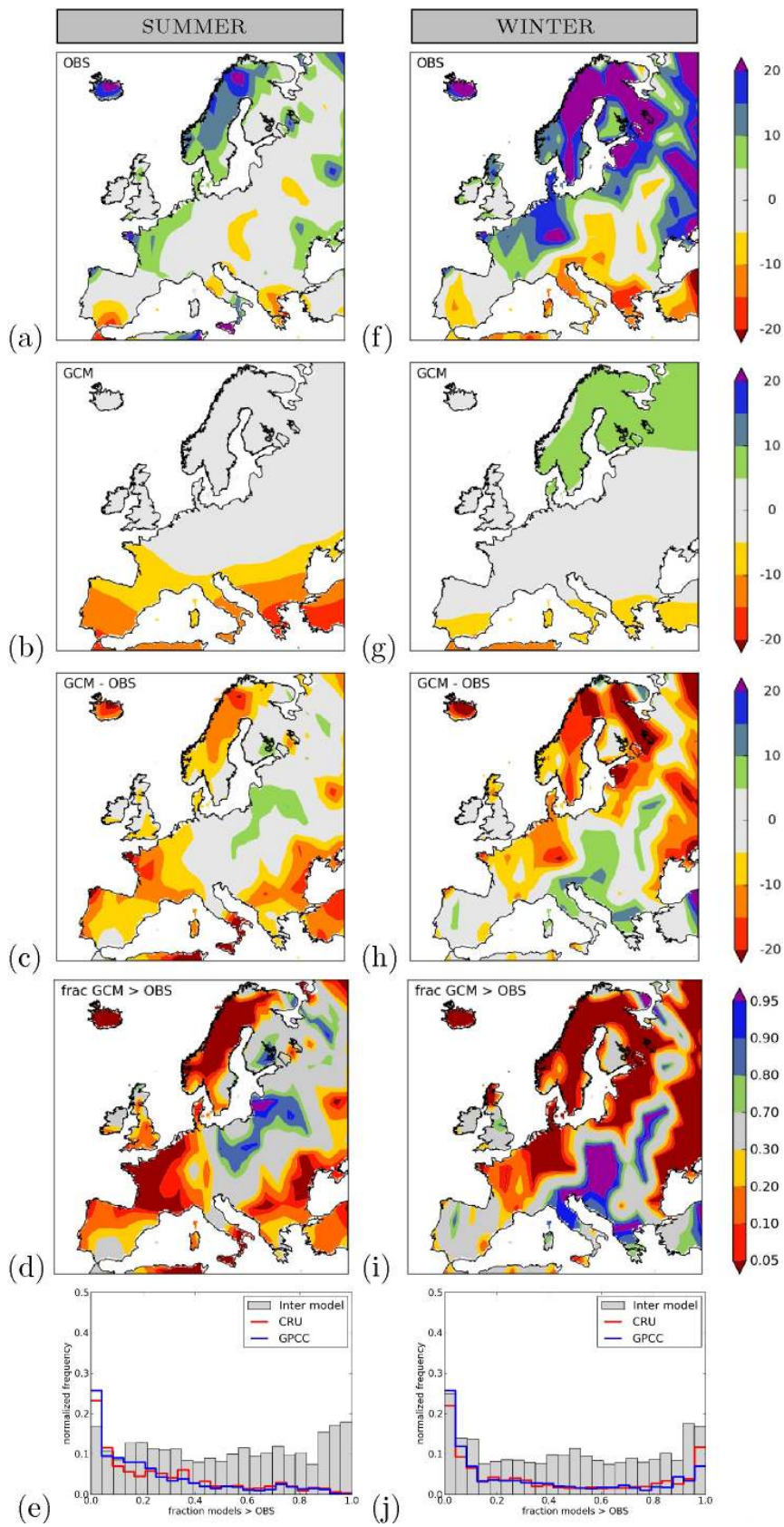
Fig. 4 Comparison of observed and GCM precipitation trends over 1901-2009, defined as the regression against time. (a) Relative trends in observed (GPCC) summer precipitation [%/Century]. (b) Mean relative trends of summer precipitation of the GCM ensemble [%/Century] (c) Bias of the GCM ensemble trend compared to the observed trend [%/Century] (d) Fraction of the GCM ensemble with trend larger than the observed one [-]. (e) Talagrand diagram (f–j) Same for winter precipitation.
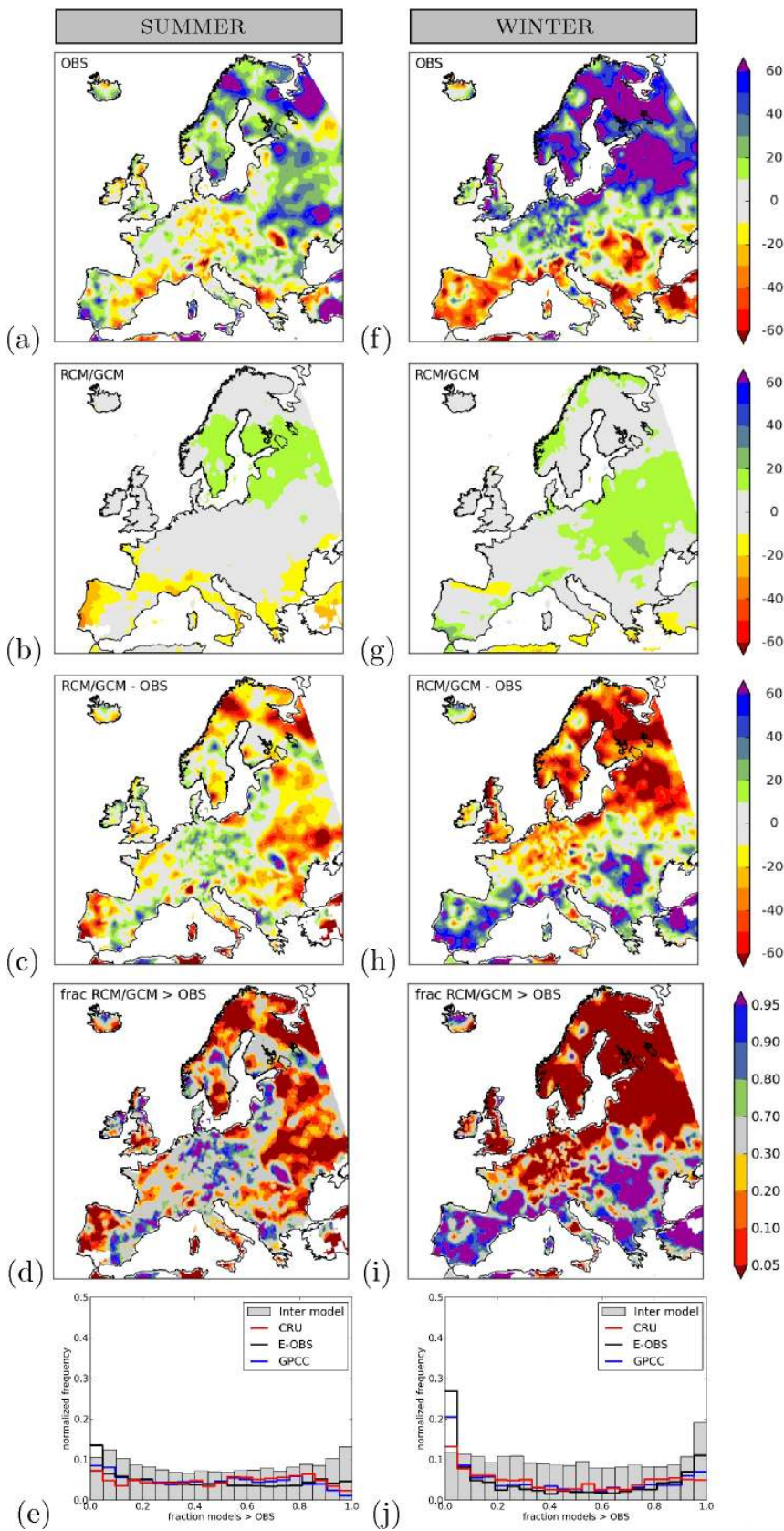
Fig. 5 Comparison of observed and GCM forced RCM precipitation trends over 1951-2009, defined as the regression against time. (a) Relative trends in observed (E-OBS) summer precipitation [%/Century]. (b) Mean relative trends of summer precipitation of the GCM forced RCM ensemble [%/Century] (c) Bias of the GCM forced RCM ensemble trend compared to the observed trend [%/Century] (d) Fraction of the GCM forced RCM ensemble with trend larger than the observed one [-]. (e) Talagrand diagram (f–j) Same for winter precipitation.
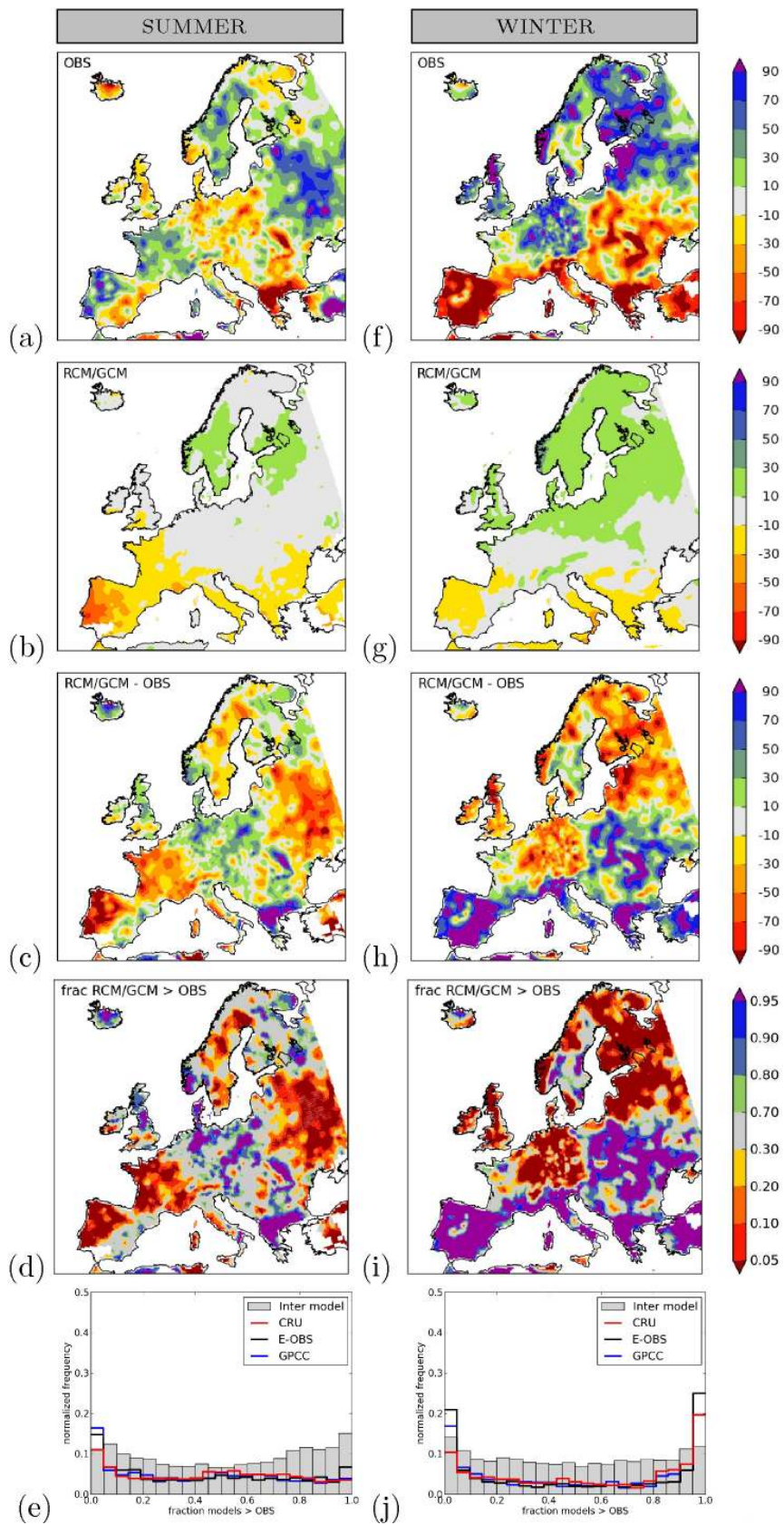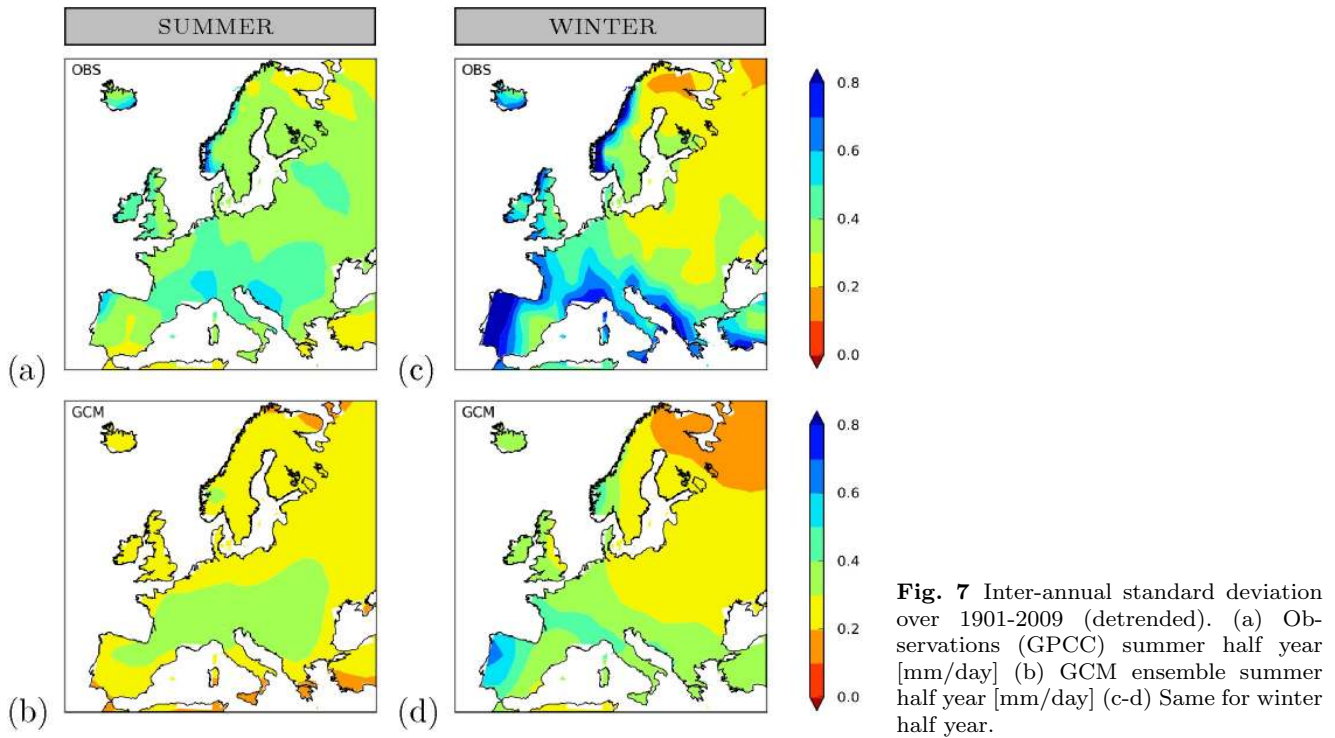
Fig. 6 Comparison of observed and GCM forced RCM precipitation trends over 1961-2000, defined as the regression against time. (a) Relative trends in observed (E-OBS) summer precipitation [%/Century]. (b) Mean relative trends of summer precipitation of the GCM forced RCM ensemble [%/Century] (c) Bias of the GCM forced RCM ensemble trend compared to the observed trend [%/Century] (d) Fraction of the GCM forced RCM ensemble with trend larger than the observed one [-]. (e) Talagrand diagram (f–j) Same for winter precipitation.

Fig. 7 Inter-annual standard deviation over 1901-2009 (detrended). (a) Observations (GPCC) summer half year [mm/day] (b) GCM ensemble summer half year [mm/day] (c-d) Same for winter half year.
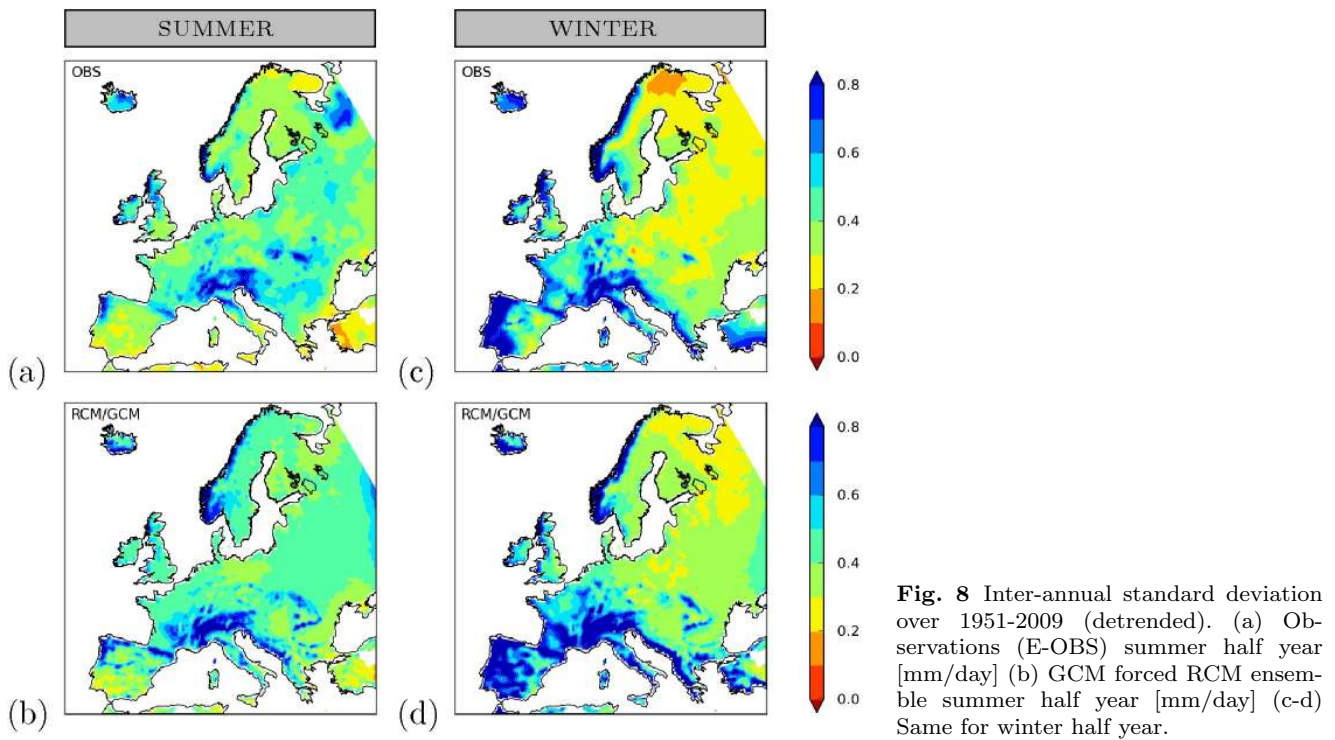
tect against the background of natural variability. Nevertheless, the modeled trends again show large biases.

For the considered time periods the observations show in the winter half year wetting trends in northern Europe and drying trends in southern Europe. Wetting trends are also observed in part of western Europe (winter half year) and northern Europe (summer half year). With the exception of slightly positive trends in parts of northern Europe (both seasons) and a small negative trend in southern Europe for the 1961-2000 period only, the GCM forced RCM ensemble fails to reproduce any of these. In fact, when considered over the same time period, the GCM ensemble shows, with the exception of details, mainly in coastal and mountainous regions, similar seasonal average trends as the GCM forced RCM ensemble (not shown).

The difference between the observed trends and modeled trends is significant in most of these areas. This is visualized in panels (d,h) of figures 5 and 6, where we show the fraction of the GCM forced RCM ensemble with a trend larger than the observed one. Note that for the GPCC observational dataset a similar spatial trend pattern is found, but often with a somewhat smaller magnitude. This is even more so for the CRU observational dataset. Especially the amount of low fractions in and around Finland differs greatly between the different observational datasets. The high fractions in southern Europe are more robust and are largely shared among the different observational datasets. Panels (e,j) show

Talagrand diagrams for the different seasons for the area west of 20° longitude, where the approximately 90% confidence interval is indicated by the gray bars. The rank histogram curls up at the low fractions in the winter half year for all observational datasets. In the summer half year they show that the models severely underestimate the observed increase in summer precipitation. This is despite the increased natural variability due to the shorter timespan considered for the GCM forced RCM ensemble.

One possible reason for the low reliability of the models would be that they underestimate the natural variability of precipitation and therefore the uncertainty in the trend. We estimated the natural variability from the same simulations as the fluctuations around the linear trend. As the autocorrelation from year to year is very small in Europe (except in southeastern Spain in winter and northern Iceland all year), and AMO teleconnections to precipitation in Europe negligible (van Oldenborgh et al., 2009b, Fig. 3d), these 60 years should give a good estimate of the fluctuations. We find that the GCMs indeed underestimate the natural variability in the precipitation trends (figure 7), but the RCMs rather overestimate the natural variability (figure 8). Note that the mean precipitation in the RCMs is, for most regions, larger than observed (not shown), slightly affecting the modeled relative precipitation trends. As a result the relative standard deviation with respect to the trend in the RCMs is smaller

Fig. 8 Inter-annual standard deviation over 1951-2009 (detrended). (a) Observations (E-OBS) summer half year [mm/day] (b) GCM forced RCM ensemble summer half year [mm/day] (c-d) Same for winter half year.

than in the observations. Nevertheless, we find that for absolute trends the modeled trends still fall outside the model spread for most regions and the overall conclusions are not affected by this.

It is unlikely that the trend biases are largely caused by either the coarse resolution of GCMs or natural variability. Because high resolution RCMs in itself are no solution for the trend biases, the remaining possibilities are that they are caused by RCM boundary conditions, large scale circulation and SST, or by local model errors present in both the RCMs and GCMs.

4 RCM simulations forced by re-analysis data

To investigate the cause of the observed trend biases in large multi-model GCM and RCM ensembles we compare the results of regional climate models with boundary conditions derived from GCMs (RT2b) with the results of a similar set of RCMs forced by quasi-observed boundary conditions (RT3). This separates the errors caused by incorrect boundary conditions from internal model errors in the RCMs (Hudson and Jones, 2002).

Figure 9 shows the results for the ERA-40 forced RCM ensemble and the E-OBS observational dataset. In general terms, the ERA-40 forced RCM ensemble reproduces much better the observed precipitation trends in both seasons than the GCM forced RCM ensemble. Wetting trends in much of northern Europe (both seasons) and in western and southwestern Europe (sum-

mer half year), as well as drying trends in southeastern (summer half year) and southern (winter half year) Europe are mostly reproduced. The Talagrand diagrams in panels (e,j) of figure 9, calculated for the area west of 20º longitude, indicate that in the summer half year the ERA-40 forced ensemble often overestimates the observed trend. In the winter half year the relative large amount of low ranks is observed for some observational datasets is largely from the Alpine region and other mountainous regions, where also the observations are uncertain.

The boundary conditions are prescribed in the ERA-40 forced RCM ensemble and are the same among the different models. Therefore, the model uncertainty in this ensemble is smaller compared to the GCM forced RCM ensemble, often resulting in a smaller spread between the different models in the ensemble. However, the Talagrand diagram in the winter half year is flatter than in figure 6 despite the smaller spread of the ensemble.

5 Simulated trends of regional climate change

Observational errors may be an important factor determining the magnitude of the observed trend on small spatial scales. Here, we will therefore look at the regional trends when aggregated over intermediate large areas. The discrepancies between modeled and observed precipitation trends are illustrated by the histograms of
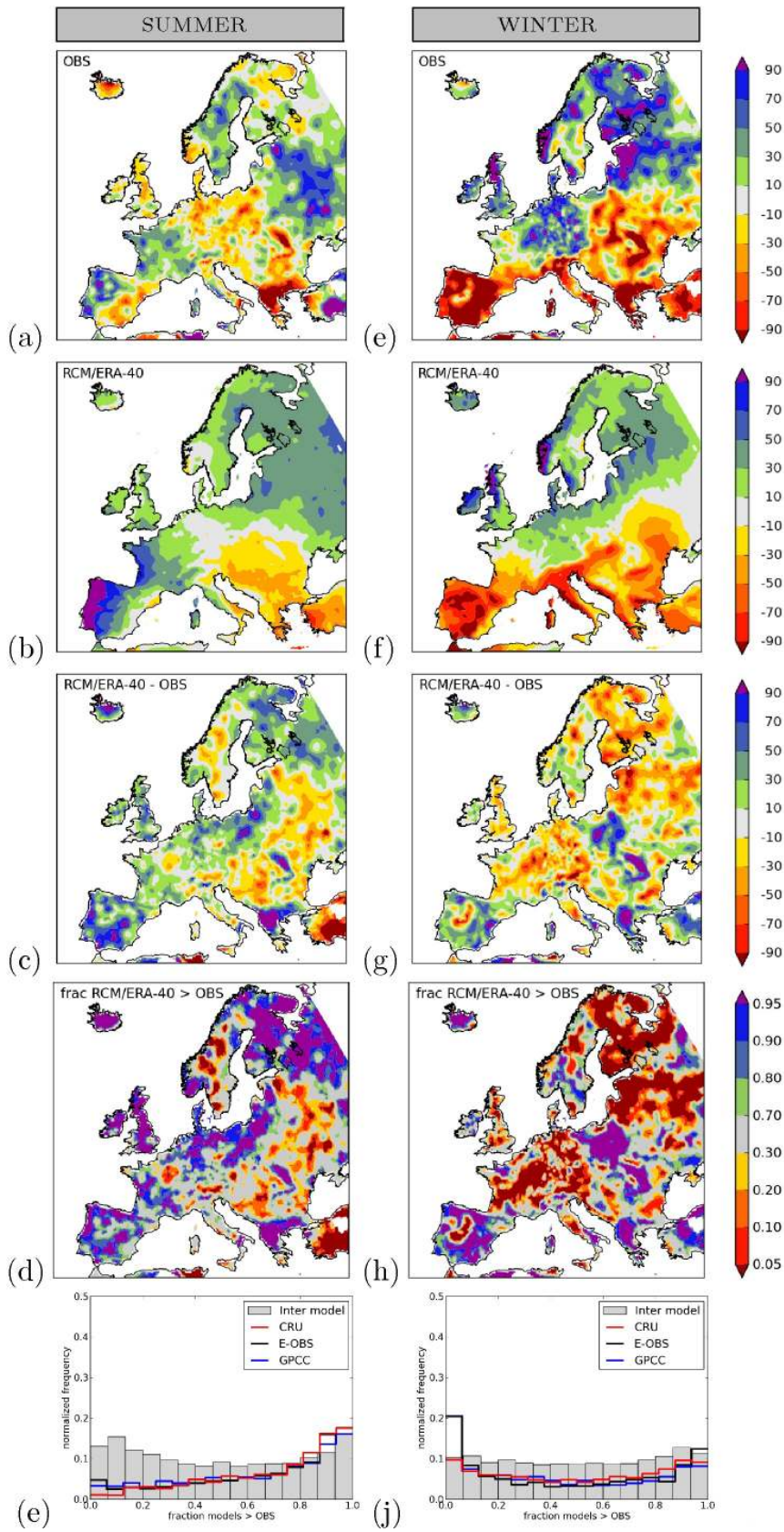
Fig. 9 Comparison of observed and ERA-40 forced RCM precipitation trends over 1961-2000, defined as the regression against time. (a) Relative trends in observed (E-OBS) summer precipitation [%/Century]. (b) Mean relative trends of summer precipitation of the ERA-40 forced RCM ensemble [%/Century] (c) Bias of the ERA-40 forced RCM ensemble trend compared to the observed trend [%/Century] (d) Fraction of the ERA-40 forced RCM ensemble with trend larger than the observed one [-]. (e) Talagrand diagram (f–j) Same for winter precipitation.

figure 11 and 12 for respectively the summer and winter half year. These show the position of the observations within the model spread for the PRUDENCE regions (see figure 10, after Christensen and Christensen (2007)). The mean trend is calculated as the trend of the average precipitation within the selected region. For illustration purposes we only consider a few specific regions and periods in the remainder of this section.
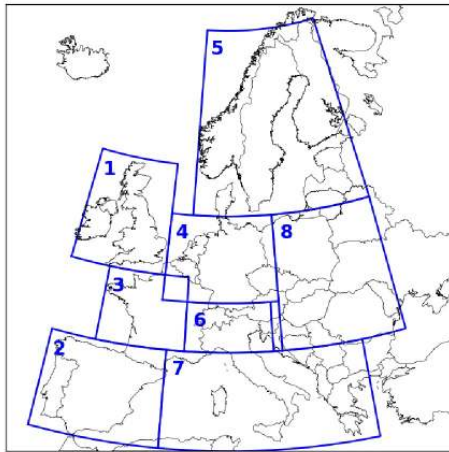

Fig. 10: PRUDENCE regions, after Christensen and Christensen (2007). (1) British Isles; (2) Iberia Peninsula; (3) France; (4) Mid-Europe; (5) Scandinavia; (6) Alps; (7) Mediterranean; (8) Eastern Europe.

To illustrate that trend biases in the RCM boundary conditions do not affect modeled precipitation trends in all regions equally, we show in panels (g,o) of figure 12 the mean relative precipitation trend for the Mid-European region for the winter half year. The means of the precipitation trends of the GCM forced and ERA-40 forced RCM ensembles are similar but the spread of the model ensemble is reduced due to the prescribed boundary conditions. Therefore, the influence of SST and atmospheric circulation trend errors on the mean precipitation trend of the ensemble in the winter half year for this region is small. Common model errors in climate models could be an explanation for the trend bias in this region, but the large spread between the different observational datasets make it difficult to determine if there indeed is a discrepancy between modeled and observed trends.

Next we show two regions where the ERA-40 forced RCM ensemble performs better compared to the GCM forced RCM ensemble. In panels (d,l) of figure 11 the mean relative precipitation trend for the France region

is shown for the summer half year. Whereas the mean of the GCM forced RCM ensemble shows a large negative trend bias, the mean of the ERA-40 forced RCM ensemble shows a (smaller) positive trend bias. In Panels (e,m) of figure 12 the mean relative precipitation trend for the Iberian Peninsula in the winter half year is shown. Whereas the ensemble spread does not cover the observations for the GCM forced RCM ensemble, it does for the ERA-40 forced RCM ensemble.

Finally we show with the British Isles for the summer half year (panels (b,j) of figure 11) a region where the trend in the observations falls within the GCM forced RCM ensemble, but is smaller than the trend in the ERA-40 forced RCM ensemble. The trend bias in local processes is hidden in the larger spread of the GCM forced RCM ensemble and can have in an opposite trend bias in the GCMs. By effectively reducing the spread of the ensemble by prescribing SST and large-scale circulation, this trend bias has become visible in panel (j) of figure 11, where the observed trend is not compatible with the ensemble spread. The better performance of the GCM forced RCM ensemble (in panel (b) of figure 11 the observed trend falls within the much wider ensemble of trends) is therefore caused by the larger spread and compensating errors in the RCMs.

It appears that prescribing realistic atmospheric flow conditions and realistic SST improves our ability to model observed trends in precipitation. Therefore, we hypothesize that the mismatch between the observations and the GCM simulations and the GCM driven RCM simulations is to a large extent due to a misrepresentation of SST and atmospheric circulation. In the next section we will investigate this further.

6 Influence of atmospheric circulation and sea surface temperature

Changes in SST and atmospheric circulation influence regional and local precipitation through convergence, evaporation and transport of moisture. Hence, in this section we investigate the influence of both large-scale circulation and SST trend biases on the precipitation trend biases in the GCM forced RCM ensemble. Changes in trend biases between the GCM forced RCM ensemble and the ERA-40 forced RCM ensemble are found in many regions. Dry trend biases in coastal regions of the North Atlantic and the North Sea are often replaced by smaller wet trend biases when realistic boundary conditions are applied. In north and south Europe the large underestimation of the trend in winter precipitation is much reduced. In Central Europe the lack of changes between the two ensembles indicate that the trends do
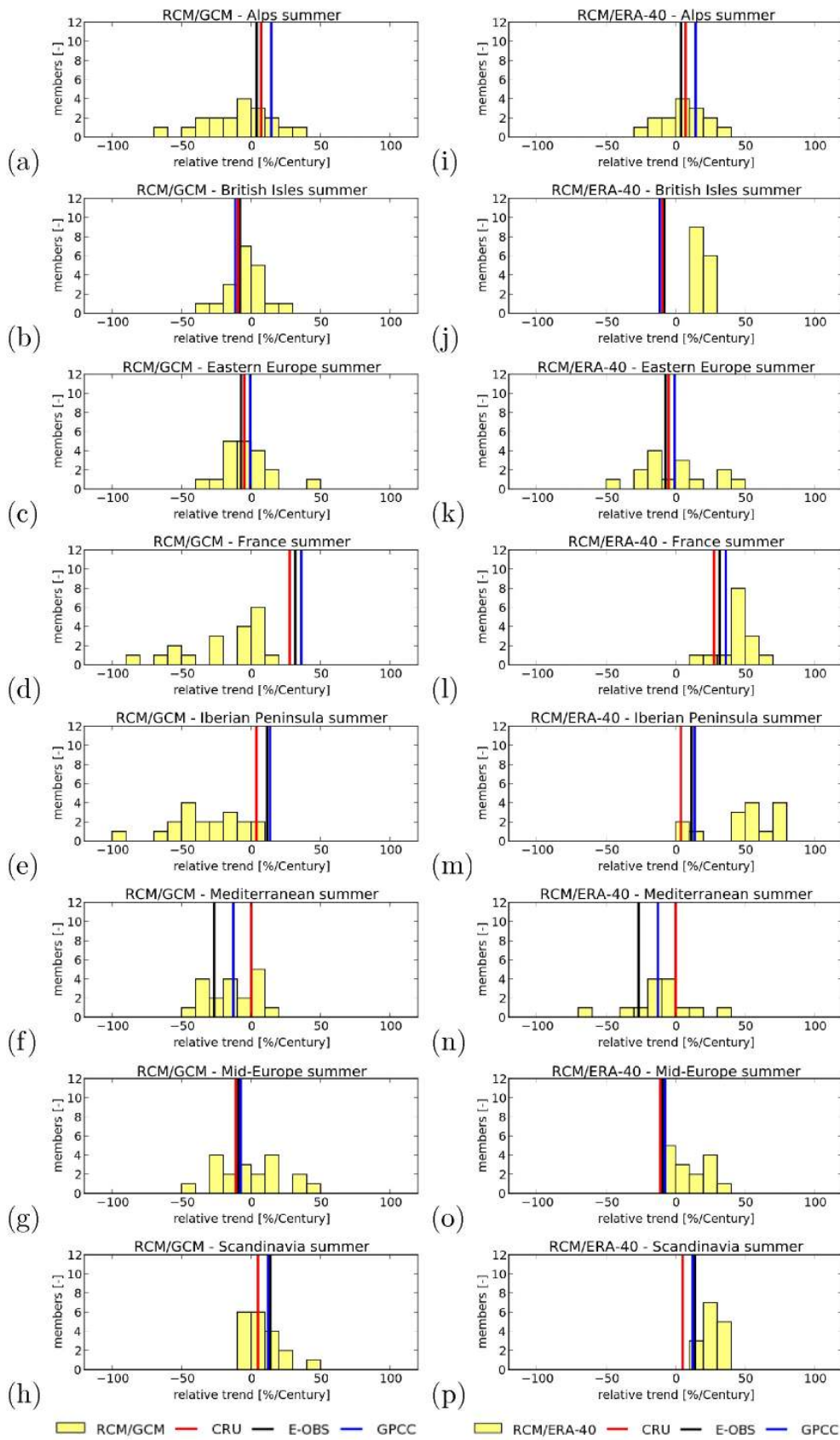
Fig. **11** Distribution of mean relative precipitation trend per region over 1961-2000 for the summer half year [%/Century].
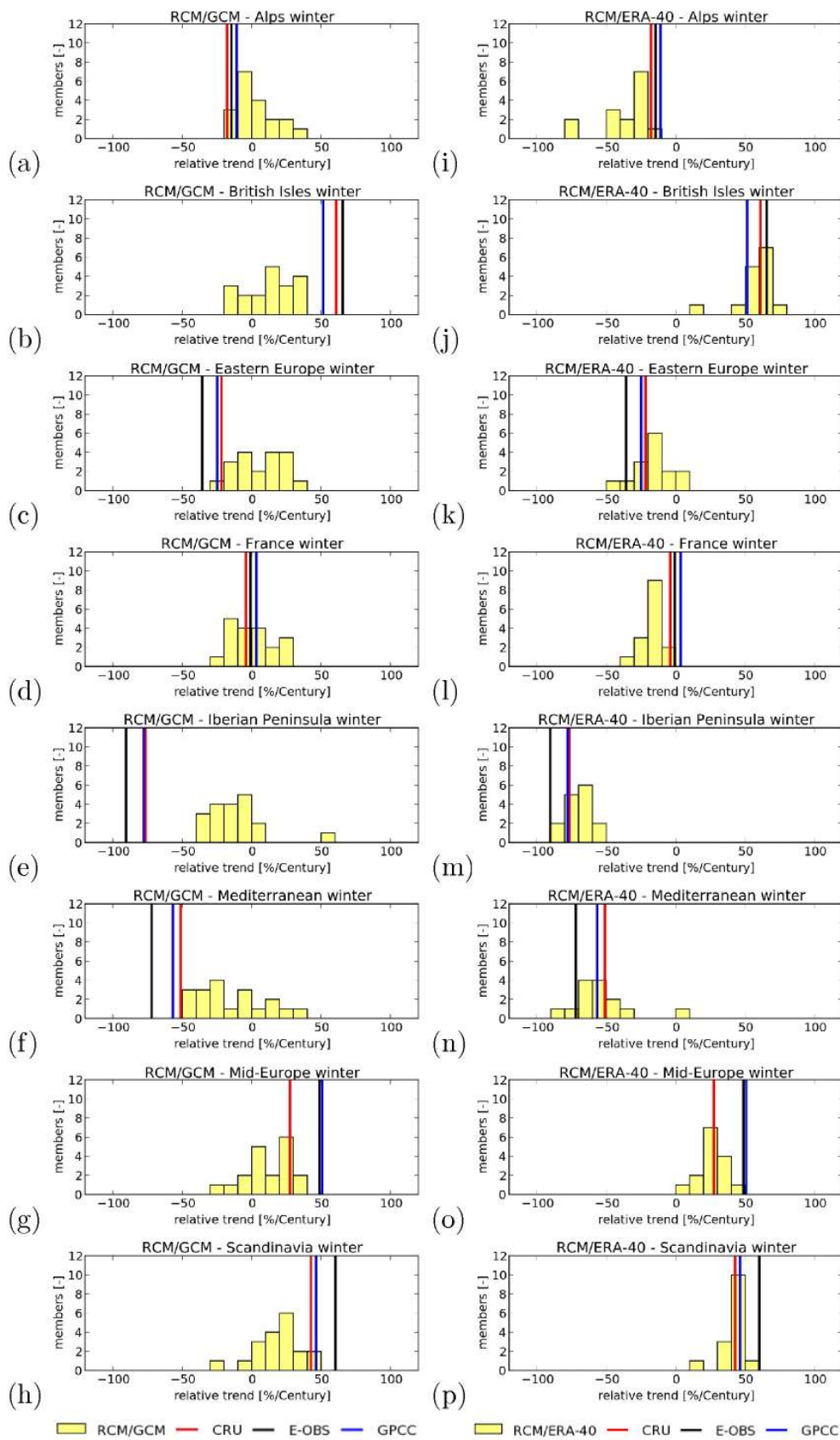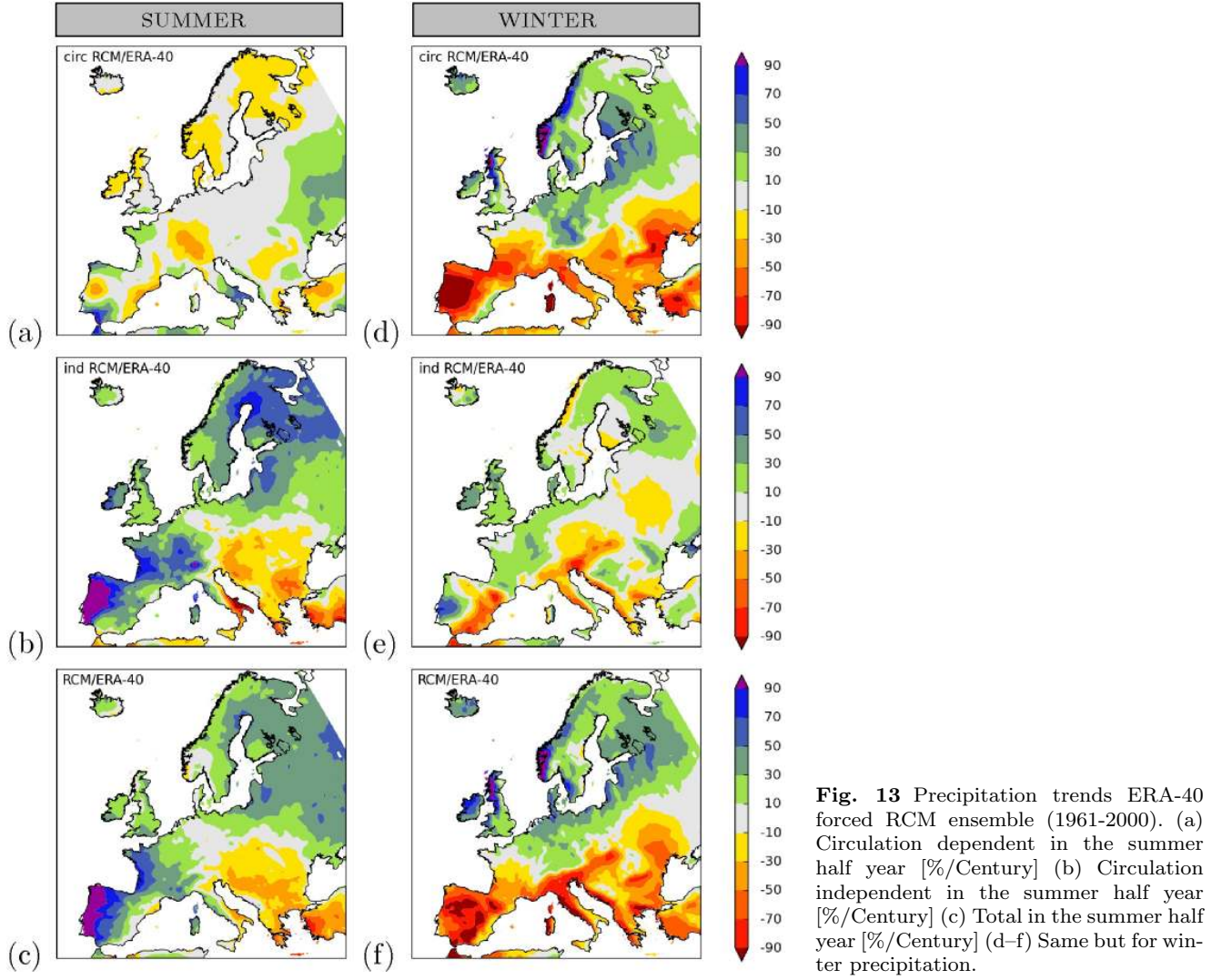
Fig. 12 Distribution of mean relative precipitation trend per region over 1961-2000 for the winter half year [%/Century].

Fig. 13 Precipitation trends ERA-40 forced RCM ensemble (1961-2000). (a) Circulation dependent in the summer half year [%/Century] (b) Circulation independent in the summer half year [%/Century] (c) Total in the summer half year [%/Century] (d–f) Same but for winter precipitation.

not strongly depend on SST and circulation trend biases.

In the winter half year (most noticeably in January – March) there has been a shift towards a more westerly circulation over Europe north of the Alps (figure 14). This change is underrepresented in climate models (Osborn, 2004; van Oldenborgh et al., 2009a). Westerlies carry moist air from the Atlantic Ocean to the continent (van Ulden and van Oldenborgh, 2006), and thereby influence the amount of precipitation. To investigate the effects of trends in the atmospheric circulation, monthly mean precipitation anomalies are approximated by a simple model that isolates the linear effect of circulation anomalies (van Ulden and van Oldenborgh, 2006; van Oldenborgh et al., 2009a). These effects include the influence of mean geostrophic wind anomalies $G'_{\mathrm{west}}(x,y,t)$, $G'_{\mathrm{south}}(x,y,t)$ and vorticity anomalies $G'_{\mathrm{vorticity}}(x,y,t)$. The other terms are the time t,

and the remaining noise $\eta(x,y,t)$:

$$P'(x,y,t) = P'_{\mathrm{circ}}(x,y,t) + P'_{\mathrm{noncirc}}(x,y,t) \qquad (3)$$

$$P'_{\mathrm{circ}}(x,y,t) = B_W G'_{\mathrm{west}}(x,y,t) + B_S G'_{\mathrm{south}}(x,y,t) \\ + B_V G'_{\mathrm{vorticity}}(x,y,t) \qquad (4)$$

$$P'_{\mathrm{noncirc}}(x,y,t) = At + \eta(x,y,t) \qquad (5)$$

The geostrophic wind anomalies $G'_{\mathrm{west}}(x,y,t)$, $G'_{\mathrm{south}}(x,y,t)$ and vorticity anomalies $G'_{\mathrm{vorticity}}(x,y,t)$ are computed from the monthly ERA-40 reanalysis sea-level pressure data and the coefficients B_W, B_S, B_V and A are fitted over 1961-2000 for each calendar month.

Atmospheric circulation induced precipitation changes show up as trends in P'_{circ}. Panels (a,d) of figure 13 show the circulation induced precipitation trend estimated by the regression model for respectively the summer and winter half year. Panels (b,e) show the
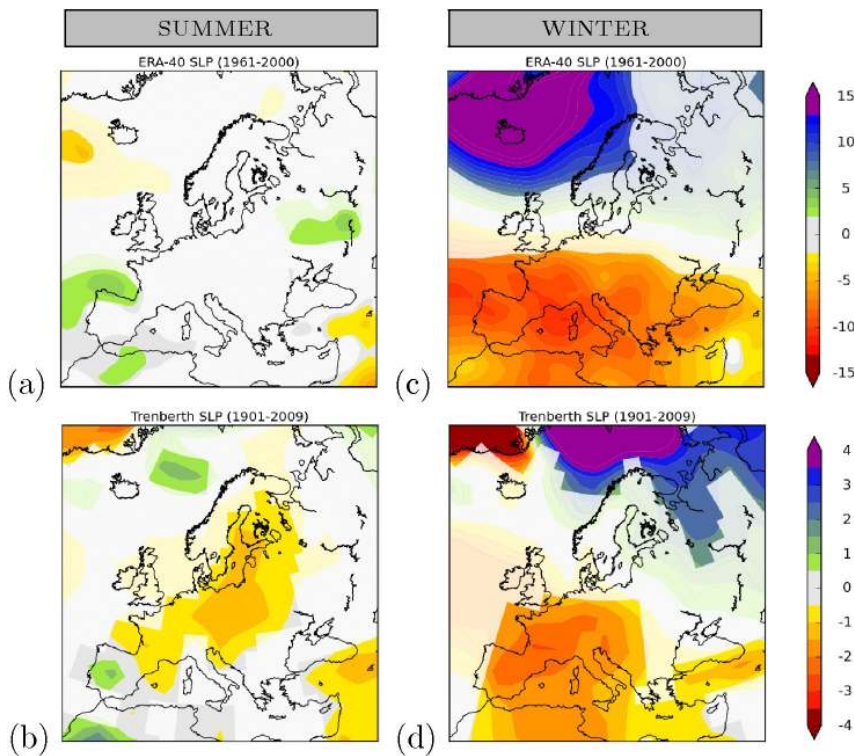
Fig. 14 Sea-level pressure trend (p < 10%) [hPa/Century]. (a) ERA-40 for 1961-2000 in the summer half year (b) Trenberth for 1901-2009 in the summer half year (c–d) Same but for winter.

circulation independent trend and panels (c,f) the total precipitation trend.

Most of the trend in summer precipitation is, within the linear approximation of a statistical decomposition, independent of circulation (figure 13b). Trends are mostly observed along the coast of the North Atlantic Ocean, the North Sea and the Baltic Sea. Because most of the trends are observed in coastal areas and are not in the GCM forced RCM ensemble, this points to a large influence of SST trend biases in the summer half year in these regions.

The oceans and seas around Europe are major sources of precipitation above Europe. Differences in SST changes affect the precipitation over Europe (Rowell, 2003; van Ulden and van Oldenborgh, 2006; Kjellström and Ruosteenoja, 2007; Lenderink et al., 2009). The modeled SST trends contain indeed biases: the GCM forced RCM ensemble underestimates the SST trends (figure 15) along the Atlantic coast and other coastal areas (if represented at all). This leads to a lower evaporation trend (not shown) and a reduced trend in coastal precipitation, even in the high-resolution RCMs. Possible explanations for the wrong SST trends in the models are a lack of resolution in the ocean component of the climate models, which causes a misrepresentation of the North Atlantic Current in the models (van Oldenborgh et al., 2009a; Ashfaq et al., 2010) and problems resolving smaller, shallow seas like the North Sea (Lenderink et al., 2009).

For most regions, a large part of the precipitation trend in the winter half year is explained by the circulation dependent part of the model (figure 13d). An increase in westerly circulation (figure 14) has resulted in an increase in precipitation in the northern part of Europe, and a decrease in the southern part of Europe (Rummukainen et al., 2004). Between 1960 - 2000 this may be partly related to a non-significant positive trend in the NAO (Bhend and von Storch, 2008), but for the other considered time periods no positive NAO trend is observed. The trend is due to a different pattern, a pressure difference between the Mediterranean and Scandinavia rather than Iceland and the Azores (van Oldenborgh et al., 2009a). The continental pressure dipole has a significant trend over all considered time periods and explains more of the variance of precipitation over most of Europe (the Ukraine is the only clear exception). In central and northern Europe and in Italy, the Mediterranean-Scandinavia pressure difference explains more variance of precipitation than the NAO, making it more suitable for analysis of precipitation trends as well (figure 16). Therefore, circulation trend biases are, under the same assumption of linearity, responsible for a large part of the underestimation of precipitation trends in northern and southern Europe in the winter half year.

Note that this analysis assumes that the effects of SST and large-scale circulation trends on the precipitation trends add linearly to the total trends. Non-linear
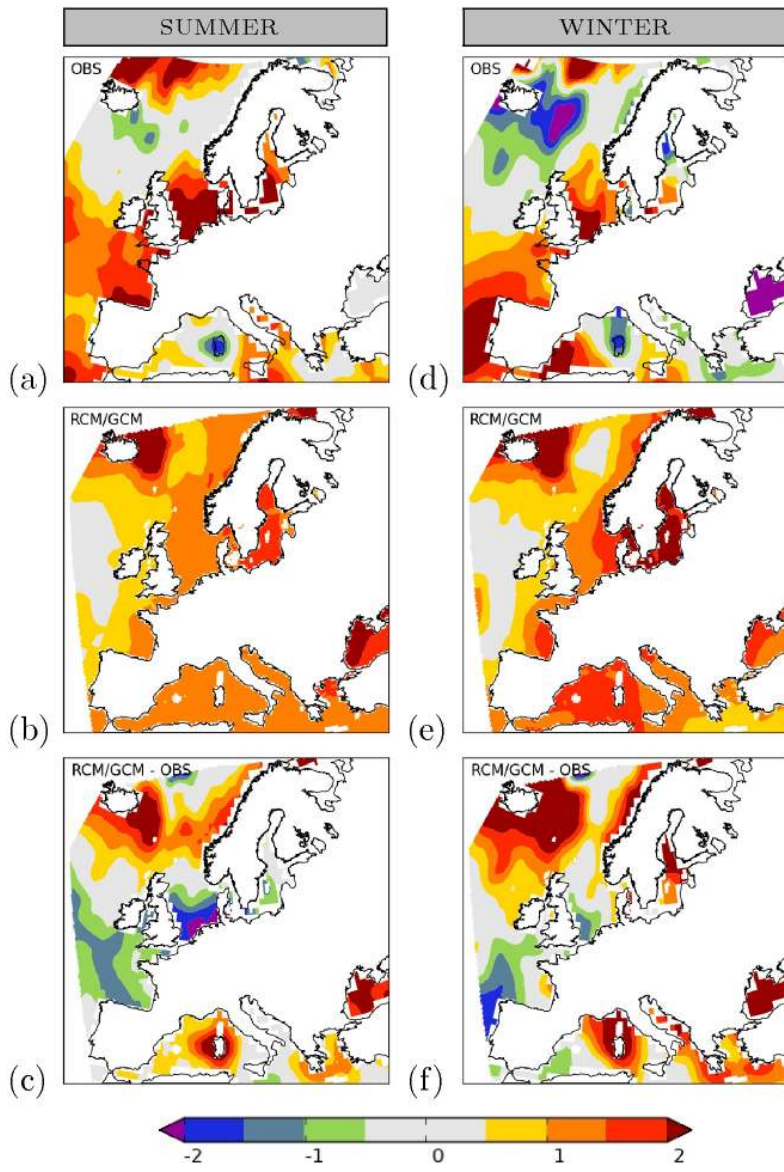
Fig. 15 Observed and modeled trends in SST over 1961-2000 [K/Century]. (a) Observed HadISST summer half year (b) RCM/GCM ensemble summer half year (c) Bias of the RCM/GCM ensemble compared to the observed trend (d-f) same but for winter half year.
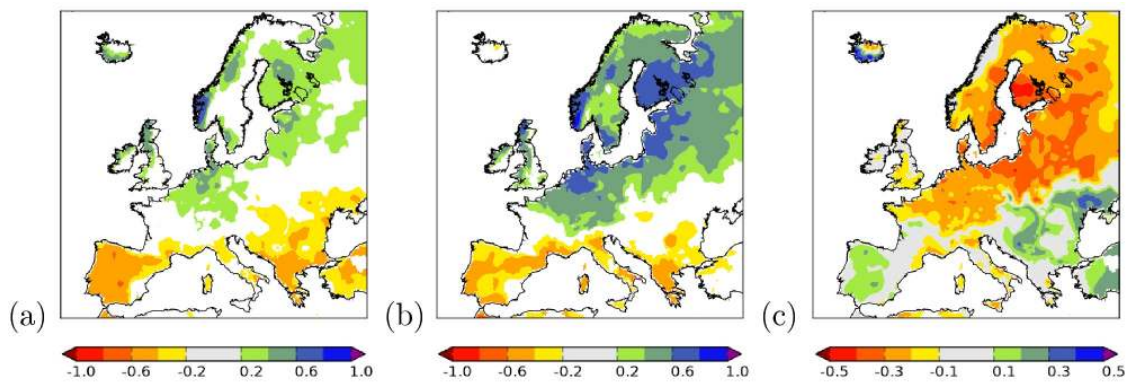

Fig. 16: Correlations of the NAO (a) and Mediterranean-Scandinavia pressure dipole (b) with local winter precipitation in Europe over 1951-2009 (p < 10%). (c) Difference in absolute correlation.

effects are not represented and may affect the conclusions.

7 Conclusions

A combination of GCMs and RCMs is often used to construct scenarios of future climate conditions. Here, the modeled precipitation trends and uncertainties over (parts of) the last century are compared to observations for a large multi-model ensemble composed of GCMs, an ensemble of RCMs forced at its boundaries by results derived from GCMs and a RCM ensemble forced by realistic, quasi-observed, boundary conditions. Such trends are relevant in, for instance, hydrological applications. A correct representation of the trend in the past is a necessary (but not sufficient) condition for confidence in future projections.

We find that modeled precipitation in GCM and GCM forced RCM ensembles contain large trend biases that fall often outside the spread of the ensemble members. A multi-model RCM ensemble forced by realistic, quasi-observed boundary conditions reproduces the observed trend much better and is largely compatible with the range of uncertainties spanned by the members of the ERA-40 forced RCM ensemble. We conclude that the boundary conditions of RCMs are responsible for large parts of the trend biases found in GCM and RCM ensembles, but are not able to explain all trend biases. The underestimation of precipitation trends in GCM forced RCM ensembles in the summer half year is mainly limited to the coastal regions and is, within the linear approximation of a statistical decomposition, largely caused by SST trend biases in the boundary conditions. The underestimation of precipitation trends in the winter half year that are observed in both northern and southern Europe are, under the same assumption of linearity, for a large part caused by circulation trend biases as present in the GCMs (van Oldenborgh et al., 2009a). This is not due to a positive trend in the NAO (Bhend and von Storch, 2008), but due to a pressure difference between the Mediterranean and Scandinavia (van Oldenborgh et al., 2009a). Remaining trend biases are likely caused by a combination of model errors in the RCMs, including land cover schemes, and errors in the observations.

To conclude, modeled atmospheric circulation and SST trends over the past century are significantly different from the observed ones. These mismatches are responsible for a large part of the misrepresentation of precipitation trends in climate models. The causes of the large trends in atmospheric circulation and summer SST are not known. For SST there may be a connection with the well-known ocean circulation biases in low-resolution ocean models. Because it is not clear (yet) whether the trend biases in SST and large scale circulation are due to greenhouse warming, their importance for future climate projections need to be determined. Therefore, a quantitative understanding of the causes of these trends is needed so that climate model based projections of future climate can be corrected for these trend biases.

Acknowledgements

References

Alexander, L. V. and J. M. Arblaster, 2009: Assessing trends in observed and modelled climate extremes over Australia in relation to future projections. *International Journal of Climatology*, **29**, 417–435, doi:10.1002/joc.1730.

Annan, J. and J. Hargreaves, 2010: Reliability of the CMIP3 ensemble. *Geophys. Res. Lett.*, doi:10.1029/2009GL041994.

Ashfaq, M., C. Skinner, and N. Diffenbaugh, 2010: Influence of SST biases on future climate change projections. *Climate Dynamics*, 1–17, 10.1007/s00382-010-0875-2.

Bhend, J. and H. von Storch, 2008: Consistency of observed winter precipitation trends in northern Europe with regional climate change projections. *Clim. Dynam.*, **31**, 17–28, doi:10.1007/s00382-007-0335-9.

Christensen, J. H. and O. B. Christensen, 2007: A summary of the PRUDENCE model projectionsof changes in European climate by the end of the century. *Climatic Change*, **81**, 7–30, doi:10.1007/s10584-006-9210-7.

Déqué, M., D. Rowell, D. Lthi, F. Giorgi, J. Christensen, B. Rockel, D. Jacob, E. Kjellström, M. de Castro, and B. van den Hurk, 2007: An intercomparison of regional climate simulations for europe: assessing uncertainties in model projections. *Climatic Change*, **81**, 53–70.

Hawkins, E. and R. T. Sutton, 2009: The potential to narrow uncertainty in regional climate predictions. *Bulletin of the American Meteorological Society*, **90**, 1095–1107, doi:10.1175/2009BAMS2607.1.

Haylock, M. R., N. Hofstra, A. M. G. K. Tank, E. J. Klok, P. D. Jones, and M. New, 2008: A European daily high-resolution gridded data set of sur-

face temperature and precipitation for 1950-2006. *Journal of Geophysical Research*, **113**, D20119+, doi:10.1029/2008JD010201.

Hegerl, G. and F. Zwiers, 2011: Use of models in detection and attribution of climate change. *Wiley Interdisciplinary Reviews: Climate Change*, doi:10.1002/wcc.121.

Hudson, D. and R. Jones, 2002: Regional climate model simulations of present-day and future climates of Southern Africa. Technical note 39, Hadley Centre for Climate Prediction and Research.

Hundecha, Y. and A. Bárdossy, 2005: Trends in daily precipitation and temperature extremes across western germany in the second half of the 20th century. *International Journal of Climatology*, **25**, 1189–1202, doi:10.1002/joc.1182.

Kjellström, E. and K. Ruosteenoja, 2007: Present-day and future precipitation in the Baltic Sea region as simulated in a suite of regional climate models. *Climatic Change*, **81**, 281–291, doi:10.1007/s10584-006-9219-y.

Knutti, R., R. Furrer, C. Tebaldi, J. Cermak, and G. A. Meehl, 2009: Challenges in Combining Projections from Multiple Climate Models. *J. Climate*, **23**, 2739–2758, doi:10.1175/2009JCLI3361.1.

Lenderink, G., E. van Meijgaard, and F. Selten, 2009: Intense coastal rainfall in the Netherlands in response to high sea surface temperatures: analysis of the event of August 2006 from the perspective of a changing climate. *Clim. Dyn.*, **32**, 19–33.

Meehl, G. A., C. Covey, T. L. Delworth, M. Latif, B. McAvaney, J. F. B. Mitchell, R. J. Stouffer, and K. E. Taylor, 2007: The WCRP CMIP3 multimodel dataset: A new era in climate change research. *Bulletin of the American Meteorological Society*, **88**, 1383–1394, doi:10.1175/BAMS-88-9-1383.

Mitchell, T. D. and P. D. Jones, 2005: An improved method of constructing a database of monthly climate observations and associated high resolution grids. *Int. J. Climatol.*, **25**, 693–712, doi:10.1002/joc.1181.

Osborn, T. J., 2004: Simulating the winter North Atlantic Oscillation: the roles of internal variability and greenhouse gas forcing. *Clim. Dynam.*, **22**, 605–623, doi:10.1007/s00382-004-0405-1.

Osborn, T. J., D. Conway, M. Hulme, J. M. Gregory, and P. D. Jones, 1999: Air flow influences on local climate: observed and simulated mean relationships for the United Kingdom. *Climate Research*, **13**, 173–191, doi:10.3354/cr013173.

Räisänen, J., 2007: How reliable are climate models? *Tellus A*, **59**, 2–29, doi:10.1111/j.1600-0870.2006.00211.x.

Rowell, D. P., 2003: The impact of Mediterranean SSTs on the Sahelian rainfall season. *Journal of Climate*, **16**, 849–862.

Rummukainen, M., S. Bergstrom, G. Persson, J. Rodhe, and M. Tjernstrom, 2004: The Swedish regional climate modelling programme, SWECLIM: a review. *Ambio*, **33**, 176–82.
URL http://highwire.stanford.edu/cgi/medline/pmid;15264

Schneider, U., T. Fuchs, A. Meyer-Christoffer, and B. Rudolf, 2010: Global precipitation analysis products of the GPCC. Technical report, Global Precipitation Climatology Centre (GPCC), Deutscher Wetterdienst, Offenbach, Germany.
URL http://gpcc.dwd.de

Turnpenny, J. R., J. F. Crossley, M. Hulme, and T. J. Osborn, 2002: Air flow influences on local climate: comparison of a regional climate model with observations over the United Kingdom. *Climate Research*, **20**, 189–202, doi:10.3354/cr020189.

van der Linden, P. and J. F. B. Mitchell, eds., 2009: *ENSEMBLES: Climate Change and its Impacts: Summary of research and results from the ENSEMBLES project*. Met Office Hadley Centre, Fitzroy Road, Exeter EX1 3PB, UK, 160pp. pp.

van der Schrier, G. and J. Barkmeijer, 2007: North American 1818–1824 drought and 1825-1840 pluvial and their possible relation to the atmospheric circulation. *Journal of Geophysical Research*, **112**, D13102+, doi:10.1029/2007JD008429.

van Oldenborgh, G. J., S. S. Drijfhout, A. P. van Ulden, R. Haarsma, C. Sterl, A. Severijns, W. Hazeleger, and H. A. Dijkstra, 2009a: Western Europe is warming much faster than expected. *Clim. Past.*, **5**, 1–12, doi:10.5194/cp-5-1-2009.

van Oldenborgh, G. J., L. A. te Raa, H. A. Dijkstra, and S. Y. Philip, 2009b: Frequency- or amplitude-dependent effects of the atlantic meridional overturning on the tropical pacific ocean. *Ocean Science*, **5**, 293–301, doi:10.5194/os-5-293-2009.

van Oldenborgh, G. J. and A. P. van Ulden, 2003: On the relationship between global warming, local warming in the Netherlands and changes in circulation in the 20th century. *Int. J. Climatol.*, **23**, 1711–1724, doi:10.1002/joc.966.

van Ulden, A. P. and G. J. van Oldenborgh, 2006: Large-scale atmospheric circulation biases and changes in global climate model simulations and their importance for climate change in Central Europe. *Atmos. Chem. Phys.*, **6**, 863–881, doi:10.5194/acp-6-863-2006.

Wentz, F. J., L. Ricciardulli, K. Hilburn, and C. Mears, 2007: How much more rain will global warming bring? *Science*, **317**, 233–235,

doi:10.1126/science.1140746.

Zhang, X., F. W. Zwiers, G. C. Hegerl, F. H. Lambert, N. P. Gillett, S. Solomon, P. A. Stott, and T. Nozawa, 2007: Detection of human influence on twentieth-century precipitation trends. *Nature*, **448**, 461–465, doi:10.1038/nature06025.